Cell type–specific channelrhodopsin-2 transgenic mice for optogenetic dissection of neural circuitry function

Shengli Zhao[1,9], Jonathan T Ting[1,2,9], Hisham E Atallah[2], Li Qiu[1], Jie Tan[3], Bernd Gloss[1,4], George J Augustine[5–7], Karl Deisseroth[8], Minmin Luo[3], Ann M Graybiel[2] & Guoping Feng[1,2]

Optogenetic methods have emerged as powerful tools for dissecting neural circuit connectivity, function and dysfunction. We used a bacterial artificial chromosome (BAC) transgenic strategy to express the H134R variant of channelrhodopsin-2, ChR2(H134R), under the control of cell type–specific promoter elements. We performed an extensive functional characterization of the newly established *VGAT-ChR2(H134R)-EYFP*, *ChAT-ChR2(H134R)-EYFP*, *Tph2-ChR2(H134R)-EYFP* and *Pvalb(H134R)-ChR2-EYFP* BAC transgenic mouse lines and demonstrate the utility of these lines for precisely controlling action-potential firing of GABAergic, cholinergic, serotonergic and parvalbumin-expressing neuron subsets using blue light. This resource of cell type–specific ChR2(H134R) mouse lines will facilitate the precise mapping of neuronal connectivity and the dissection of the neural basis of behavior.

Optogenetic strategies for controlling neuronal function are being widely implemented for dissecting neural connectivity, function and dysfunction. To this end, it is crucial to target optogenetic constructs to defined neuronal subsets within complex brain circuits. A variety of approaches including *in utero* electroporation[1,2] and *in vivo* injections of viral vectors[3–18] have been used to gain important insights into mammalian nervous system function using channelrhodopsin-2 (ChR2). These gene delivery methods can prove labor-intensive and technically challenging, and there are several important limitations. Every experimental mouse requires surgical stereotaxic delivery of virus encoding the *ChR2* transgene. Inevitably, not every injected mouse is suitable for experimentation owing to experimenter error. Even the mice deemed suitable may have variable spread of the virus at the injection site, gradients of transgene expression in infected brain regions or potential tissue damage. These potential confounding factors are eliminated in cell type–specific *ChR2* transgenic mouse lines, and the availability of such lines to the neuroscience community would greatly facilitate progress in this burgeoning field.

We had previously generated *ChR2* transgenic mouse lines (*Thy1-ChR2-EYFP* lines 9 and 18) with ChR2 fused to enhanced YFP (EYFP) expressed in subsets of neurons throughout the nervous system[19,20]. These lines have been used in a variety of studies[10,13]. Subsequent studies have reported additional transgenic rodent lines, including *Thy1.2-ChR2-Venus* rats with expression in retinal ganglion cells[21], *Vglut-ChR2(H134R)-EYFP* mice with expression in spinal cord and hindbrain[22], *OMP-ChR2-EYFP* mice with expression in olfactory sensory neurons[23], and *αCaMKII-tTA::BTR6* mice with expression of ChR2-mCherry in striatal medium spiny neurons (MSNs)[24]. Collectively, these lines enable optogenetic control of some defined neuronal cell types, though clearly additional lines are required to access the diverse classes of neurons and circuits throughout the nervous system.

Here we used a BAC transgenic strategy to express ChR2 (H134R)-EYFP under the control of cell type–specific promoters to enable functional activation of GABAergic, cholinergic, serotonergic and parvalbumin (Pvalb)-expressing neuronal populations with blue light. Our mouse lines have robust and functional transgene expression in defined populations of neurons that is stable in terms of both pattern and amount of ChR2-EYFP expression across generations.

RESULTS

VGAT-ChR2(H134R)-EYFP transgenic mice

The vesicular γ-aminobutyric acid (GABA) transporter (VGAT) is specifically expressed in GABAergic neurons and glycinergic neurons[25,26]. To express ChR2(H134R)-EYFP in these inhibitory neurons, we targeted *ChR2(H134R)-EYFP* to exon I of *Slc32a1* (here referred to as *VGAT*) (**Supplementary Fig. 1**). Note that we used the *ChR2(H134R)* mutant gene to generate all lines in this work but throughout the results refer to it as *ChR2* and call the encoded ChR2(H134R) protein ChR2.

Four of ten founder lines had a virtually indistinguishable ChR2-EYFP expression pattern throughout the brain, though

[1]Department of Neurobiology, Duke University Medical Center, Durham, North Carolina, USA. [2]McGovern Institute for Brain Research and Department of Brain and Cognitive Sciences, Massachusetts Institute of Technology, Cambridge, Massachusetts, USA. [3]National Institute of Biological Sciences, Beijing, China. [4]Duke NeuroTransgenic Laboratory, Duke University Medical Center, Durham, North Carolina, USA. [5]Center for Functional Connectomics, Korea Institute of Science and Technology, Seoul, Republic of Korea. [6]Program in Neuroscience and Behavioral Disorders, Duke–National University of Singapore Graduate Medical School, Singapore. [7]Agency for Science, Technology and Research, Duke–National University of Singapore Neuroscience Research Partnership, Singapore. [8]Department of Bioengineering, Stanford University, California, USA. [9]These authors contributed equally to this work. Correspondence should be addressed to G.F. (fengg@mit.edu).

RECEIVED 17 MARCH; ACCEPTED 14 JULY; PUBLISHED ONLINE 7 AUGUST 2011; DOI:10.1038/NMETH.1668

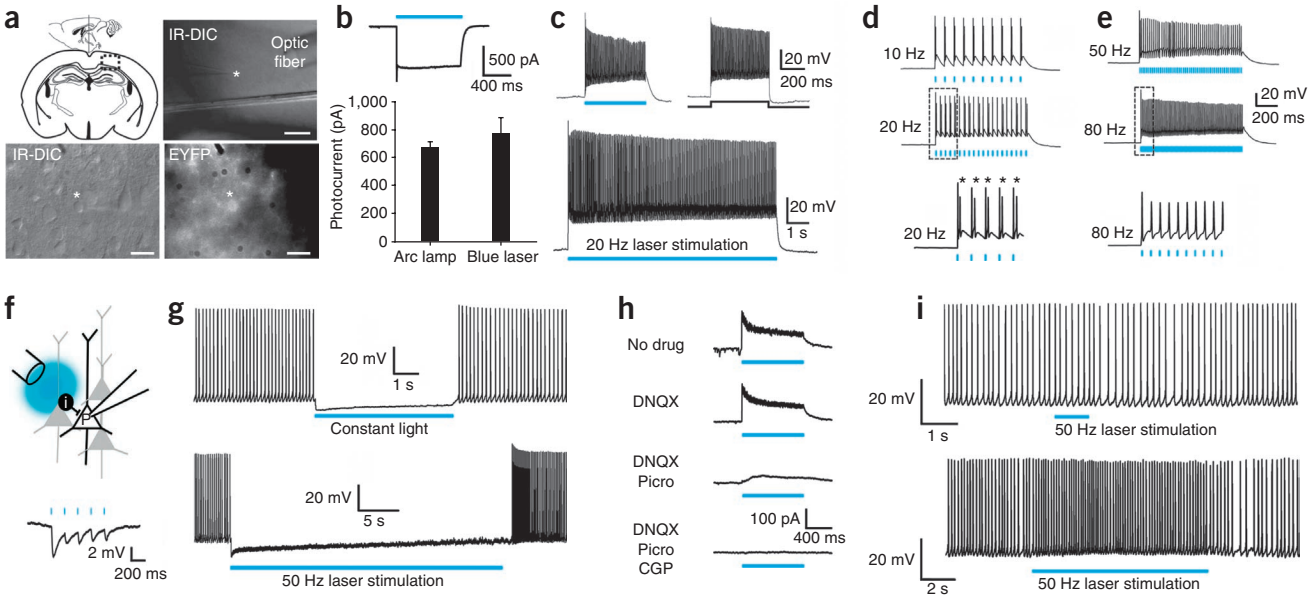

Figure 1 | Functional characterization of *VGAT-ChR2(H134R)-EYFP* BAC transgenic mice. (**a**) Diagram of acute coronal brain slice preparation containing the cortex and representative image from the boxed region showing placement of the optic fiber in the region of recorded cortical interneurons (asterisk) (top). Scale bar, 200 µm. High-magnification infrared differential interference contrast (IR-DIC) image and EYFP fluorescence image of a layer V interneuron (bottom). Scale bars, 20 µm. (**b**) Voltage-clamp recording with stimulation by blue laser light (blue line, 26.3 mW mm^{-2}) (top). Plot of peak steady-state photocurrent in response to indicated light (bottom). Error bars, mean ± s.e.m.; arc lamp (constant blue light), n = 12 neurons; blue laser, n = 7 neurons. (**c**) Current clamp mode recording showing firing of a single neuron in response to blue light (blue line, top left), +400 pA current injection (top right) or prolonged 20-Hz stimulation (0.52 mW mm^{-2}, 1 ms pulse width; bottom). (**d**) Current clamp mode recording showing action potential firing in response to patterned blue laser light (2.1 mW mm^{-2}, 1 ms pulse width) (top and middle). An expanded view of initial action potential firing at 20 Hz reveals extra spikes (asterisks; bottom). (**e**) Current clamp mode recording showing action potential firing of the same interneuron to patterned blue laser light (2.1 mW mm^{-2}, 1 ms pulse width) (top and middle). Expanded view of firing at 80 Hz is shown (bottom). (**f**) Diagram of recording configuration to test functional effect of light-induced interneuron firing in cortical microcircuits (top). Current clamp mode recording of a layer V pyramidal neuron showing hyperpolarization in response to 5-Hz blue laser light (2.1 mW mm^{-2}, 1 ms pulse width) (bottom). (**g**) Layer V pyramidal neuron activity upon stimulation with constant blue light (top) or 50-Hz blue laser stimulation (473 nm, 2.1 mW mm^{-2}, 1 ms pulse width) (bottom). Action potential firing was induced by constant +150 pA direct current injection. (**h**) Voltage clamp recording of the same layer V pyramidal neuron in the absence (no drug) and presence of 6,7-dinitroquinoxaline-2,3-dione (DNQX), picrotoxin (Picro) and (2*S*)-3-(((1*S*)-1-(3,4-dichlorophenyl) ethyl)amino-2-hydroxypropyl)(phenylmethyl)phosphinic acid hydrochloride (CGP). Blue bars indicate 50-Hz blue laser stimulation. (**i**) Response of the same neuron to 50-Hz blue laser light (2.1 mW mm^{-2}, 1 ms pulse width) for 1 s (top) or 10 s (bottom) during simultaneous application of GABA-A and GABA-B receptor antagonists.

with variable expression. We characterized the *VGAT-ChR2-EYFP* line 8 because it showed the strongest ChR2-EYFP expression (**Supplementary Table 1**). Whole-brain sagittal images revealed strong ChR2-EYFP expression in the glomerular and mitral cell layer of the olfactory bulb, thalamic reticular nucleus (TRN), superior and inferior colliculus, the molecular layer of cerebellum and brain stem. We also detected moderate ChR2-EYFP expression in the cortex, hippocampus, thalamus and the granule cell layer of the olfactory bulb (**Supplementary Fig. 2a** and **Supplementary Fig. 3a–k**). Combined immunostaining of GAD67 and EYFP revealed co-localization of these proteins throughout the brain (**Supplementary Fig. 2b–d**). Co-localization of GAD67-immunopositive neurons with ChR2-EYFP was 93% in the cortex, 93% in the hippocampus, 88.6% in the inferior colliculus and 100% in Purkinje cells. The vast majority of the ChR2-EYFP–expressing neurons were GAD67-immunopositive (**Supplementary Table 2**), suggesting the ChR2-EYFP–expressing neurons in this line were indeed inhibitory neurons.

To confirm that ChR2 in the *VGAT-ChR2-EYFP* line was functional, we performed electrophysiological recordings of neuronal activity and membrane currents in acute brain slices from young adult mice. We identified cortical interneurons for electrophysiological recordings by visualization of EYFP fluorescence at the somata (**Fig. 1a**). Delivery of blue light through an optic fiber positioned just above the recorded neurons elicited robust photocurrents (**Fig. 1b**). In the current-clamp mode, a 1-s blue light stimulus caused high-frequency repetitive action-potential firing with no accommodation in the majority of recorded cortical interneurons, suggesting that these were putative fast-spiking interneurons. Subsequent analysis revealed that these cortical interneurons sustained high-fidelity, high-frequency firing in response to prolonged bouts of patterned blue light stimulation at 20 Hz (**Fig. 1c**). We next assessed the fidelity of action-potential firing across a range of blue laser stimulation frequencies. At low frequencies, the neurons responded with reliable action-potential firing, but we commonly observed extra spikes (**Fig. 1d**), which previously has been shown to be due to slow off kinetics of the wild-type and H134R variant of ChR2 (ref. 27). We observed fewer extra spikes as we increased stimulation frequency, and the majority of ChR2-expressing cortical interneurons fired action potentials with near perfect fidelity at 80 Hz (**Fig. 1e**).

To address the functionality of the ChR2 in the context of local cortical circuitry, we recorded from cortical layer V pyramidal

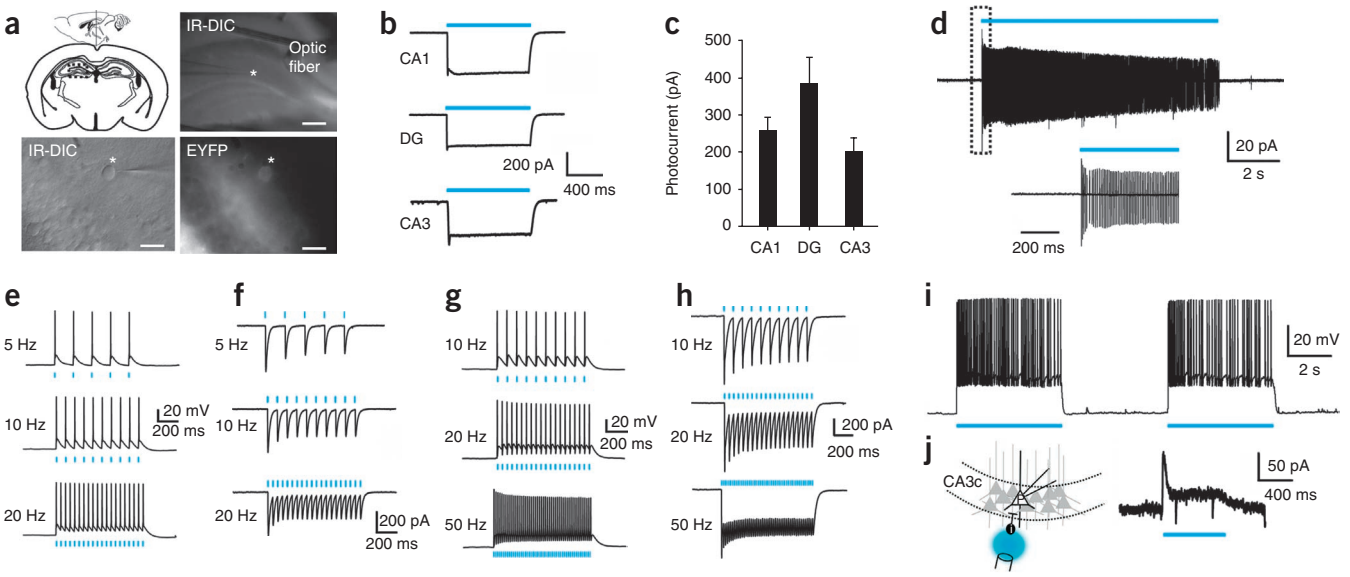

Figure 2 | Functional characterization of hippocampal interneurons in *VGAT-ChR2(H134R)-EYFP* BAC transgenic mice. (**a**) Diagram of acute coronal brain slice preparation containing the hippocampus and representative image from the boxed region showing placement of the optic fiber in the region of a recorded hippocampal interneuron (asterisk) (top). Scale bar, 200 µm. High-magnification IR-DIC and fluorescence image (EYFP) of an interneuron in the dentate gyrus molecular layer (bottom). Scale bars, 20 µm. (**b**) Example photocurrents induced by blue laser light (blue lines; 26.3 mW mm^{-2}) in various hippocampal regions. DG, dentate gyrus. (**c**) Plot of peak steady-state photocurrent in response to blue light for interneurons in various hippocampal regions. Error bars, mean ± s.e.m.; CA1 region, n = 11 neurons; DG region, n = 7 neurons; CA3 region, n = 6 neurons. (**d**) Cell-attached recording of a dentate gyrus interneuron demonstrating firing in response to 10-s constant blue light stimulation (inset, expanded view). (**e**,**f**) Current clamp (**e**) and voltage clamp (**f**) mode recording of a dentate gyrus interneuron in response to patterned blue laser (2.1 mW mm^{-2}, 1 ms pulse width). (**g**,**h**) Current clamp (**g**) and voltage clamp (**h**) mode recording of a CA1 interneuron response to patterned blue laser light (2.1 mW mm^{-2}, 1 ms pulse width). (**i**) Current clamp mode recording of a CA3 interneuron showing sustained action potential firing in response to repeated bouts of constant blue light. (**j**) Diagram of recording configuration to test functional effect of light-induced interneuron firing in the CA3c subfield circuitry (left) and voltage clamp recording of a CA3c pyramidal neuron demonstrating outward current in response to blue light (right).

neurons that did not express ChR2. By constant current injection, we caused pyramidal neurons to fire repetitively and applied blue light to the surrounding region to activate nearby ChR2-expressing interneurons (**Fig. 1f**). Cortical neuron firing was strongly suppressed by constant blue light or pulse trains of blue light at 50 Hz (**Fig. 1g**). Acute application of various synaptic blockers demonstrated that the inhibition of pyramidal-neuron firing required activation at both GABA-A and GABA-B receptors (**Fig. 1h**,**i**).

We extended our functional analysis of *VGAT-ChR2-EYFP* line 8 to hippocampal interneurons identified by bright EYFP fluorescence at the somata (**Fig. 2a**). All recorded hippocampal interneurons exhibited robust photocurrents (**Fig. 2b**,**c**) and the vast majority also fired action potentials in response to blue light. Interneurons in the CA1 and dentate gyrus regions responded with high fidelity to blue light up to 20 Hz (**Fig. 2d**–**f**), and some interneurons in CA1 fired action potentials in response to patterned blue light at frequencies up to 50 Hz (**Fig. 2g**,**h**). CA3 interneurons fired continuously in response to prolonged constant blue light (**Fig. 2i**), and this firing produced synaptic hyperpolarizing current recorded from CA3 pyramidal neurons (**Fig. 2j**). These results demonstrate broad functional ChR2 expression in local inhibitory interneurons distributed throughout the cortex and hippocampus. We also observed light-evoked GABA release from axon terminal fields in the medial habenula that originate from putative long-range GABAergic projection neurons of the medial septum and nucleus of the diagonal band[28] (**Supplementary Figs. 4** and **5**).

ChAT-ChR2(H134R)-EYFP transgenic mice

Choline acetyltransferase (ChAT) is the enzyme responsible for acetylcholine synthesis. We targeted *ChR2(H134R)-EYFP* (called *ChR2-EYFP* throughout) to the initiating ATG codon in exon III of *Chat* (here referred to as *ChAT*). Three of eighteen founder lines exhibited ChR2(H134R)-EYFP expression in the brain (**Supplementary Table 1**). *ChAT-ChR2-EYFP* line 6 showed strong ChR2-EYFP expression in the striatum, basal forebrain, facial nucleus, trochlear nucleus, medial habenula, interpeduncular nucleus (IPN) and various other brainstem motor nuclei (**Supplementary Figs. 6** and **7**). We observed low ChR2-EYFP expression in the cortex and hippocampus. Immunostaining using antibodies to ChAT and to GFP revealed strong co-localization in cortex (100%), striatum (100%), globus pallidus (100%) and medial habenula (98.2%) (**Supplementary Fig. 6b**–**d** and **Supplementary Table 2**), confirming the cholinergic identity of ChR2-EYFP–expressing neurons.

We targeted striatal cholinergic neurons for electrophysiological recordings in acute brain slices from adult *ChAT-ChR2-EYFP* line 6 transgenic mice based on their characteristic large somata and membrane targeted ChR2-EYFP fluorescence (**Fig. 3a**). The majority of recorded neurons exhibited a characteristic tonic firing and pronounced hyperpolarization activated currents (I_h)[29]. Blue light elicited robust photocurrents that in some neurons exceeded 1 nA, indicating very strong ChR2 expression (**Fig. 3b**). Consequently, these neurons fired action potentials in response to patterned light up to 20 Hz (**Fig. 3c**). Firing became less reliable at frequencies above 20 Hz (data not shown). Owing to the powerful

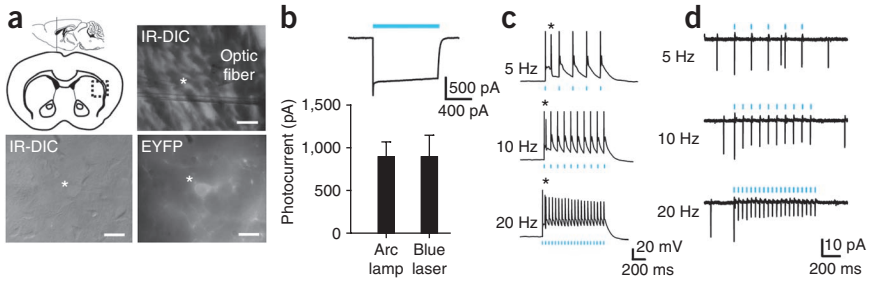

Figure 3 | Functional characterization of *ChAT-ChR2(H134R)-EYFP* line 6 BAC transgenic mice. (**a**) Diagram of acute coronal brain slice containing the dorsal striatum and a representative image from the boxed region showing placement of the optic fiber in the region of a recorded neuron (top). Scale bar, 200 µm. IR-DIC and EYFP fluorescence image of a recorded striatal cholinergic neuron (bottom). Scale bars, 20 µm. (**b**) Voltage clamp recording demonstrating inward current induced by blue laser light (26.3 mW mm^{-2}) (top). Summary plot of peak steady-state photocurrent in response to blue light (bottom). Error bars, mean ± s.e.m.; arc lamp, n = 5 neurons; blue laser, n = 5 neurons. (**c**) Action potential firing in response to patterned blue laser light (5.21 mW mm^{-2}, 5 ms pulse width). Asterisks indicate extra spikes. A small hyperpolarizing current injection was applied to silence basal firing. (**d**) Cell-attached recording of firing in response to patterned blue laser light (2.1 mW mm^{-2}, 5 ms pulse width). Light stimuli were delivered on top of basal tonic firing.

abrupt depolarization with light, many neurons exhibited extra spikes after the first elicited action potential in the train (**Fig. 3c**). 'Cell-attached' recordings (a less invasive configuration in which the cell membrane at the recording electrode tip is not ruptured) demonstrated that precisely timed action potentials could readily be induced on top of spontaneous tonic firing (**Fig. 3d**).

Next we investigated the functional activation of striatal cholinergic neurons in *ChAT-ChR2-EYFP* line 6 mice *in vivo* by implanting tetrodes together with an optic fiber for simultaneous electrophysiological recording of neural activity and delivery of precisely patterned blue laser stimulation in awake, behaving mice. We identified putative striatal cholinergic neuron units by their characteristic tonic spiking activity. A single pulse of blue light delivered over hundreds of identical repeated trials evoked highly reliable spiking (**Fig. 4a**). The putative striatal cholinergic neurons exhibited low basal tonic spiking at 3–5 Hz in the absence of photostimulation, and 30-Hz blue-light pulses robustly potentiated the basal spiking (**Fig. 4b**). The measured firing frequency slightly exceeded 30 Hz owing to the presence of extra spikes, consistent with the data obtained in acute slice recordings. The laser stimulation did not affect our ability to cluster individual neurons based on the differences in waveform shape and size (**Supplementary Fig. 8**), and the light-induced spiking exhibited a rapid response onset of 1–2 ms (**Fig. 4c**), indicating a direct response to blue laser stimulation. The capacity to drive spiking with 30-Hz patterned blue light over tens of seconds demonstrated the high reliability of firing that can be achieved *in vivo* and provides evidence that the dynamic range for modulating neuronal firing rates may be broader *in vivo* compared to *in vitro*.

We examined the influence of striatal cholinergic neuron activity on putative MSN units in striatal circuits *in vivo*. When we stimulated cholinergic neurons with 30-Hz blue laser light, putative MSNs showed decreased firing frequency (**Fig. 4d**; 'light-off' trials, 0.65 Hz and 'light-on' trials, 0.33 Hz). This finding closely matches the results obtained in a recent study that used virus-mediated delivery of ChR2(H134R)-EYFP to modulate striatal cholinergic neuron activity *in vivo*[16]. Our findings demonstrate the utility of *ChAT-ChR2-EYFP* line 6 for analysis of complex circuitry in awake, behaving mice.

In *ChAT-ChR2-EYFP* line 6 brain slices we frequently observed that striatal cholinergic neurons entered a state of 'depolarization block' of action-potential firing with prolonged light presentation, presumably because of strong depolarization induced by ChR2 activation. In light of this observation, we also characterized a lower-expressing line, *ChAT-ChR2-EYFP* line 5, which had no visible EYFP fluorescence in striatal cholinergic neurons in live slices despite strong signal with immunostaining with an antibody to GFP. Nevertheless, stimulation with blue light reliably elicited clear photocurrents (**Supplementary Fig. 9a**). These responses were an order of magnitude lower than the average responses measured for the same neuronal population in line 6, but this low ChR2 expression was sufficient to drive robust potentiation of action potential firing in response to sustained blue light (**Supplementary Fig. 9b**,**c**). The potentiation of firing rate

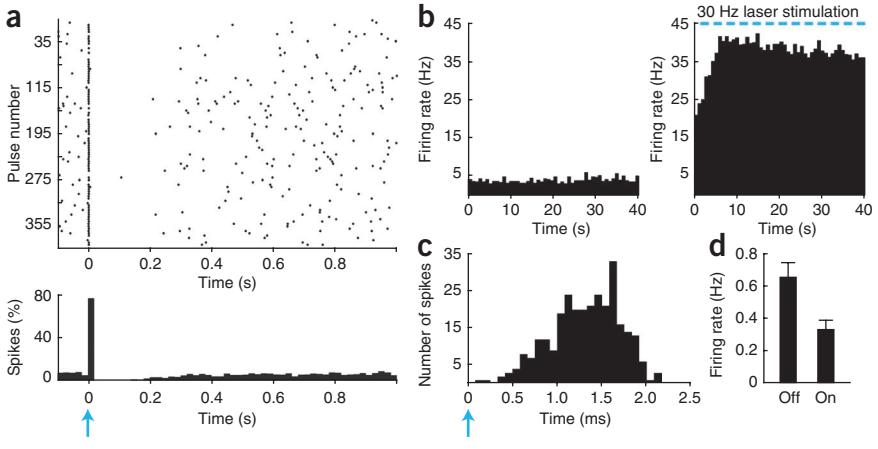

Figure 4 | *In vivo* striatal electrophysiology for *ChAT-ChR2(H134R)-EYFP* line 6 BAC transgenic mice. (**a**) Raster (top) and spike-density histograms (bottom) of a striatal cholinergic neuron in response to a single pulse of blue laser light (10 mW, 18 ms pulse width, blue arrow) over repeated trials. (**b**) Spike-density histogram of a striatal cholinergic neuron in response to 40 s of 30-Hz blue laser light stimulation (10 mW, 18 ms pulse width). (**c**) Spike-density histogram of a striatal cholinergic neuron showing rapid response (1–2 ms) to blue laser light (10 mW, 18 ms pulse width, blue arrow). (**d**) Bar graph of putative medium spiny neuron firing rate in response to 40 s of 30-Hz blue laser light stimulation (10 mW, 18 ms pulse width). Error bars, mean ± s.e.m.; n = 20 units, $P < 0.01$).

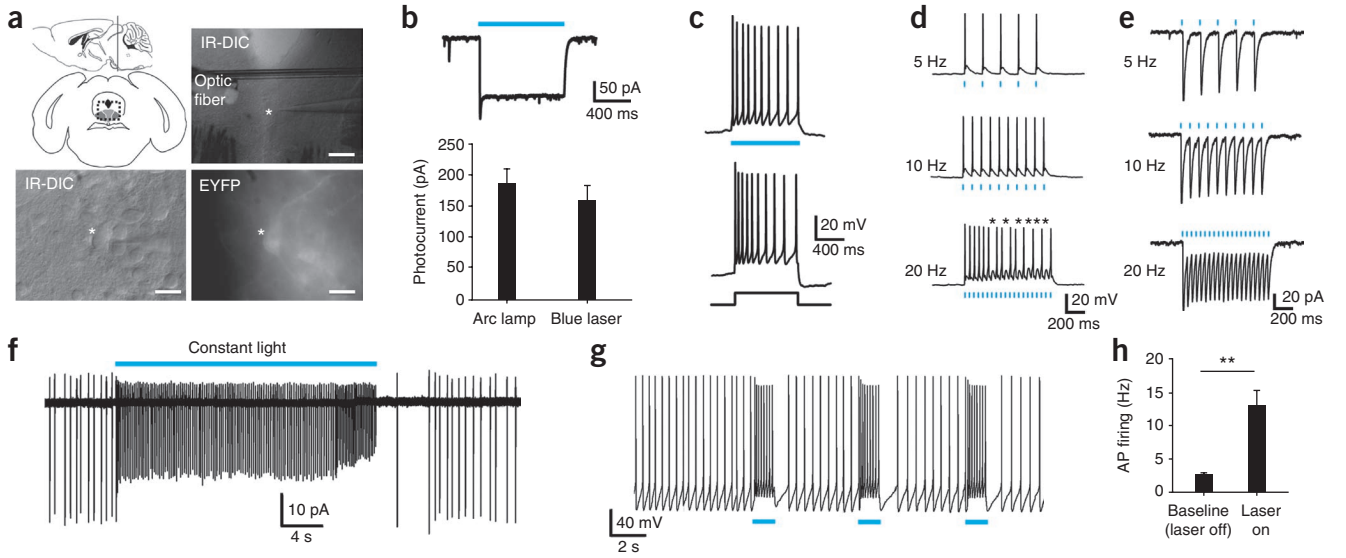

Figure 5 | Functional characterization of *TPH2-ChR2(H134R)-EYFP* BAC transgenic mice. (**a**) Diagram of acute coronal brainstem slice preparation and representative image from the boxed region showing placement of the optic fiber in the region of a recorded neuron (top). Scale bars, 200 µm. IR-DIC and EYFP fluorescence image of a recorded serotonergic neuron in the dorsal raphe nucleus (bottom). Scale bars, 20 µm. (**b**) Voltage clamp recording of a serotonergic neuron demonstrating inward current induced by blue laser light (26.3 mW mm^{-2}) (top). Plot of peak steady-state photocurrent in response to blue light delivered as indicated (bottom). Error bars, mean ± s.e.m.; arc lamp, $n = 11$ neurons; blue laser, $n = 9$ neurons. (**c**) Current clamp mode recording showing action potential firing in response to blue laser light (26.3 mW mm^{-2}) (top) or in response to +100 pA current injection (bottom). (**d**–**e**) Current clamp mode (**d**) and voltage clamp (**e**) recording of responses to patterned blue laser light (26.3 mW mm^{-2}, 5 ms pulse width). Asterisks indicate missed action potentials. A small hyperpolarizing current injection was applied (**c**,**d**) to silence basal firing. (**f**,**g**) Cell-attached recording of a serotonergic neuron under prolonged constant blue light stimulation (**f**) or to repeated bouts of blue light (**g**). (**h**) Summary plot of baseline and blue light-induced firing rates. AP, action potential. Error bars, mean ± s.e.m.; laser-off and laser-on conditions, $n = 5$ neurons; $^{**}P < 0.01$ (one-tailed paired *t*-test).

could be sustained for 30 s or longer in many recorded neurons (**Supplementary Fig. 9d**). These data demonstrate that *ChAT-ChR2-EYFP* line 5 may be useful for potentiation of basal firing with blue light over tens of seconds, whereas *ChAT-ChR2-EYFP* line 6 will be more useful when precisely timed firing in response to blue-light pulses is desirable. In addition, we found that *ChAT-ChR2-EYFP* line 6 (but not line 5) should be useful for axon-stimulation experiments using blue light as we demonstrated for the medial habenula to IPN projection pathway (**Supplementary Figs. 10** and **11**).

TPH2-ChR2(H134R)-EYFP transgenic mice

The enzyme tryptophan hydroxylase 2 (TPH2) is the rate-limiting enzyme in the synthesis of serotonin (or 5-hydroxytryptamine; 5-HT) in the central nervous system. We engineered *ChR2(H134R)-EYFP* (called *ChR2-EYFP* throughout) into the ATG site of the first exon of *Tph2* (here referred to as *TPH2*). Only one of six founder lines had adequate ChR2-EYFP expression in the brainstem (**Supplementary Table 1**). We observed moderate ChR2-EYFP expression in the dorsal raphe nucleus (DRN), median raphe nucleus (MnR) and IPN (**Supplementary Fig. 12**). TPH2 immunofluorescence strongly localized with signal for GFP antibody–labeled neurons (81% for DRN, 87.1% for MnR and 85% for IPN), confirming the serotonergic identity of ChR2-EYFP–expressing neurons in this line (**Supplementary Fig. 12** and **Supplementary Table 2**). The ChR2-EYFP–expressing neurons were virtually all TPH2-positive (100% for DRN and MnR, and 98.5% for IPN), which suggests that ChR2-EYFP was selectively expressed in serotonergic neurons with no ectopic expression.

We performed electrophysiological recordings of ChR2-EYFP–expressing neurons in the DRN in acute brain slices from juvenile mice. The serotonergic neurons were identified by their large polymorphic somata, location in the DRN and EYFP fluorescence at the soma. In many serotonergic neurons we could visualize brightly fluorescent segments of neuronal processes (**Fig. 5a**). Recorded neurons routinely exhibited basal tonic firing in our acute slice preparation (mean, 2.63 Hz), similar to rates recorded *in vivo*[30,31].

Recorded DRN serotonergic neurons responded to blue light with moderate amplitude photocurrents (mean, 158.8 pA; **Fig. 5b**). In the current-clamp mode, we evoked a nearly identical action potential firing pattern in response to either a short blue light pulse or a +100 pA current injection step (**Fig. 5c**). Reliable action potential firing could be evoked from DRN serotonergic neurons at up to 20 Hz with patterned blue light, although we observed missed spikes late in the train for some neurons (**Fig. 5d**,**e**). We observed variability in the ChR2-EYFP expression across the many sampled DRN serotonergic neurons. In particular, in some putative serotonergic neurons we did not see EYFP fluorescence in the live slices. These neurons responded with very weak photocurrents, thus confirming their identity as serotonergic neurons yet with low functional ChR2-EYFP expression (**Supplementary Fig. 13**). Thus, we focused on characterizing the subpopulation of serotonergic neurons with visible EYFP fluorescence. We found that basal tonic firing could be potentiated by short bouts of blue light in a consistent and repeatable manner, and by sustained presentation of blue light up to tens of seconds (**Fig. 5f**–**h**). We also found that patterned photostimulation could over-ride basal tonic firing (**Supplementary Fig. 13**).

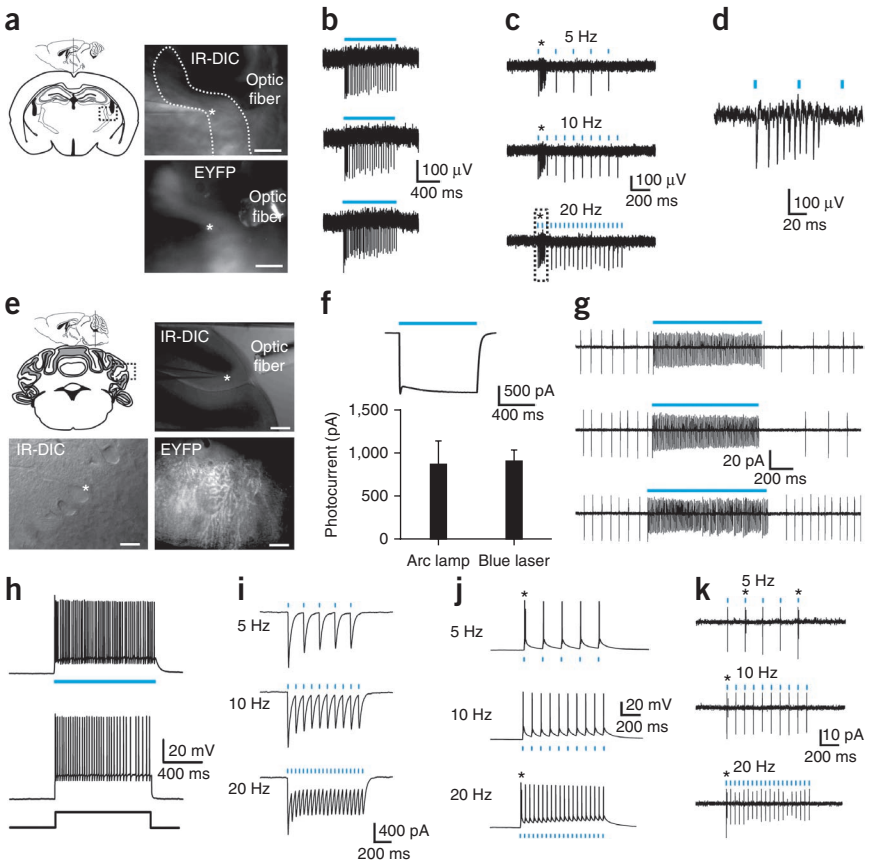

Figure 6 | Functional characterization of *Pvalb-ChR2(H134R)-EYFP* BAC transgenic mice. (**a**) Diagram of a coronal brain slice containing the TRN and representative image from the boxed region showing placement of the optic fiber (top) and EYFP fluorescence (bottom) in the region of recorded neurons. Scale bars, 200 µm. (**b**) Extracellular field recordings of a putative single TRN neuron that was silent at rest in response to blue laser light at 10.5 mW mm^{-2} (top) and 26.3 mW mm^{-2} (middle), or delivered from a mercury arc lamp (bottom). (**c**) Extracellular field recording of action potential firing in response to patterned blue laser light (26.3 mW mm^{-2}, 5 ms pulse width). Asterisks indicate initial burst firing. (**d**) Expanded view of the bottom recording in **c**. (**e**) Diagram of an acute brain slice containing the cerebellum and representative slice image from the boxed region showing placement of the optic fiber in the region of a recorded neuron in the Purkinje cell layer (top). Scale bar, 200 µm. IR-DIC image and EYFP fluorescence image of a recorded Purkinje cell (bottom). EYFP fluorescence was not easily detected in the Purkinje cell somata owing to saturating EYFP fluorescence of the Purkinje cell dendrites in the adjacent molecular layer. Scale bars, 20 µm. (**f**) Voltage clamp recording demonstrating inward current induced by blue laser light (26.3 mW mm^{-2}) (top). Summary plot of peak steady-state photocurrent in response to blue light delivered as indicated (bottom). Error bars, mean ± s.e.m.; arc lamp, $n = 5$ neurons; blue laser, $n = 10$ neurons. (**g**) Cell-attached recordings demonstrating potentiation of baseline firing in response to blue laser light at 1.05 mW mm^{-2} (top), 26.3 mW mm^{-2} (middle) and 157.9 mW mm^{-2} (bottom). (**h**) Current clamp mode recording showing firing in response to blue light (top) or to +400 pA current injection (bottom). (**i**,**j**) Voltage clamp (**i**) and current clamp mode (**j**) recordings demonstrating responses to patterned blue laser light (26.3 mW mm^{-2}, 5 ms pulse width). Asterisks indicate initial doublet firing. A small hyperpolarizing current injection was applied to silence basal firing. (**k**) Cell-attached recording of action potential firing from a single neuron in response to patterned blue laser light (26.3 mW mm^{-2}, 5-ms pulse width). Asterisks indicate doublet firing. This recorded Purkinje cell was silent at rest.

Pvalb-ChR2(H134R)-EYFP transgenic mice

To selectively express ChR2 in Pvalb-expressing interneurons, we targeted *ChR2(H134R)-EYFP* (called *ChR2-EYFP* throughout) to the ATG codon in exon II of *Pvalb*. Six of ten founder lines exhibited detectable ChR2-EYFP expression with nearly identical patterns in the brain (**Supplementary Table 1**). We selected *Pvalb-ChR2-EYFP* line 15 for analysis; this line had strong expression throughout the molecular layer of the cerebellum, the TRN and brainstem, and low expression in the thalamus and inferior colliculus (**Supplementary Fig. 14a**). Immunostaining with antibodies to parvalbumin and GFP confirmed that these ChR2-EYFP–expressing neurons were parvalbumin-expressing interneurons (**Supplementary Fig. 14b**,**c**). Despite the known expression of parvalbumin in cortical, striatal and hippocampal interneuron subsets, we observed no functional ChR2-EYFP expression in these areas, likely reflecting the relatively weak activity of the parvalbumin promoter in these regions.

We performed electrophysiological recordings in acute brain slices from adult *Pvalb-ChR2-EYFP* mice. We performed extracellular field recordings of putative TRN units located in the area bounded by clear EYFP fluorescence (**Fig. 6a** and **Supplementary Fig. 14a**). TRN units responded to constant blue light with a complex pattern of firing consisting of an initial burst of spikes followed by simple spiking (**Fig. 6b**–**d**) that is the predominant characteristic firing pattern of this neuron type[32,33]. Patterned light stimulation also elicited initial burst firing, but the simple spiking portion of the response exhibited perfect fidelity up to the maximum tested frequency of 20 Hz (**Fig. 6c**).

Pvalb-ChR2-EYFP mice also exhibited very strong EYFP fluorescence in the molecular layer of the cerebellum, suggesting this line may be useful to control neuronal firing in cerebellar circuitry. Thus, we identified Purkinje cells for electrophysiological recordings based on their characteristic large somata, prominent apical dendrite and laminar organization in the Purkinje cell layer. In live slices, we observed bright EYFP fluorescence throughout the Purkinje cell dendritic tree (**Fig. 6e**) but not at the somata. These neurons exhibited large inward photocurrents in response to blue light (mean, 900.0 pA; **Fig. 6f**). In many Purkinje cells we evoked sustained action potential firing with constant blue light (**Fig. 6g**,**h**), and there was a marked similarity of the action potential firing pattern in response to either a short blue light pulse or a +400 pA current-injection step (**Fig. 6h**). Purkinje cells reliably fired action potentials in response to patterned blue laser stimulation up to 20 Hz (**Fig. 6i**–**k**). Over the frequencies tested we rarely observed missed spikes but often observed extra spikes after the initial action potential in a train (**Fig. 6j**,**k**).

The extra spikes are most likely due to the rapid and pronounced depolarization with light resulting from high ChR2 expression or prolonged depolarization after each spike. The powerful depolarization upon ChR2 activation at high laser power was sufficient to induce complex spikes in a subset of Purkinje cells (**Fig. 6g**). The complex spikes consisted of initial simple spikes with superimposed tetrodotoxin-insensitive putative dendritic Ca^{2+} spikes (**Supplementary Fig. 15a**), and these observations are consistent with known active properties of Purkinje cell dendrites[34].

DISCUSSION

The use of cell type–specific *ChR2(H134R)-EYFP* transgenic mouse lines is a simple alternative to costly and labor-intensive methods for repeated *ChR2* delivery to several broad classes of mammalian central nervous system neurons. Continued efforts along these lines will be valuable for enabling optogenetics-based investigations for the many diverse classes of neurons and circuits throughout the mammalian nervous system.

A recent study described a Cre recombinase–inducible *ChR2-EGFP* knock-in mouse and used this line to analyze the organization of cortical interneuron connectivity in neocortical circuits[35]. To achieve functional *ChR2-EGFP* expression it was necessary to use mice homozygous for the inducible *ChR2* allele and heterozygous for a transgene directing expression of tamoxifen-inducible *Cre* in cortical interneurons, demonstrating that this line confers only weak Cre recombinase–inducible ChR2 expression. These findings closely match data obtained with a virtually identical mouse line previously developed in our laboratory using the ChR2(H134R) variant (unpublished data). Additional modifications to the strategy, such as those recently implemented for creating improved *Cre* reporter mice[36], will be required to achieve robust ChR2 expression from a broadly applicable Cre recombinase–inducible knock-in allele. Furthermore, we empirically found that the optimal ChR2 expression necessary to achieve dynamic functional manipulation of neuron firing can vary extensively across diverse neuron types, and thus, it may not be possible to achieve optimal ChR2 expression in all neuron types with a single generic inducible *ChR2* knock-in allele.

Our BAC transgenic strategy achieves the same cell-type specificity as inducible *ChR2* alleles combined with *Cre* driver lines but does not require complicated breeding schemes. These transgenic mice will be particularly desirable for investigators using ChR2 to elucidate and potentially correct circuitry dysfunction in existing genetic mouse models of neurological disorders. In such existing models, a substantial increase in the complexity of the breeding schemes or delivery techniques for introduction of ChR2 may be prohibitive. Thus, the tools we developed greatly simplify the experimental paradigms needed to perform optogenetics-based investigations of circuitry function for several important classes of central nervous system neurons and will make these approaches widely accessible to scientists exploring a diverse range of topics in neurobiology.

METHODS

Methods and any associated references are available in the online version of the paper at http://www.nature.com/naturemethods/.

Note: Supplementary information is available on the Nature Methods website.

ACKNOWLEDGMENTS

We thank P. Miao, K. Harley, L. Strickland and J. Chemla for technical assistance with mouse husbandry and genotyping, Q. Liu and members of the NeuroTransgenic lab at Duke University for pronuclear injections of BAC DNA and other members of the Feng laboratory for their support, C. Keller-McGandy for help with histology in the Graybiel lab, and J. Ren and other members of the Luo lab for providing electrophysiology expertise and input. This work was supported by an American Recovery and Reinvestment Act grant from the US National Institute of Mental Health (RC1-MH088434) to G.F., a National Alliance for Research on Schizophrenia and Depression: The Brain and Behavior Research Foundation Young Investigator award and US National Institutes of Health Ruth L. Kirschstein National Research Service award (F32MH084460) to J.T.T. and a National Institute of Mental Health grant to A.M.G. (R01 MH060379).

AUTHOR CONTRIBUTIONS

G.F., K.D. and G.J.A. initiated the project. K.D. provided *ChR2(H134R)* DNA constructs. S.Z., L.Q. and B.G. generated the *ChR2* BAC transgenic founder lines. S.Z. and L.Q. screened the founder lines. S.Z. performed all confocal imaging experiments. J.T.T. performed electrophysiological recordings, and analyzed and interpreted acute-brain-slice experiments for all mouse lines. J.T. performed electrophysiological recordings, and M.L. and J.T. analyzed and interpreted acute brain slice experiments on *ChAT-ChR2(H134R)-EYFP* line 6 and *VGAT-ChR2(H134R)-EYFP* line 8 mice. H.E.A. performed *in vivo* electrophysiology, and H.E.A. and A.M.G. analyzed and interpreted *in vivo* electrophysiology data on *ChAT-ChR2(H134R)-EYFP* line 6 mice. J.T.T. and G.F. wrote the manuscript.

COMPETING FINANCIAL INTERESTS

The authors declare no competing financial interests.

Published online at http://www.nature.com/naturemethods/.
Reprints and permissions information is available online at http://www.nature.com/reprints/index.html.

1. Gradinaru, V. *et al.* Targeting and readout strategies for fast optical neural control in vitro and in vivo. *J. Neurosci.* **27**, 14231–14238 (2007).
2. Huber, D. *et al.* Sparse optical microstimulation in barrel cortex drives learned behaviour in freely moving mice. *Nature* **451**, 61–64 (2008).
3. Johansen, J.P. *et al.* Optical activation of lateral amygdala pyramidal cells instructs associative fear learning. *Proc. Natl. Acad. Sci. USA* **107**, 12692–12697 (2010).
4. Adamantidis, A.R., Zhang, F., Aravanis, A.M., Deisseroth, K. & de Lecea, L. Neural substrates of awakening probed with optogenetic control of hypocretin neurons. *Nature* **450**, 420–424 (2007).
5. Bi, A. *et al.* Ectopic expression of a microbial-type rhodopsin restores visual responses in mice with photoreceptor degeneration. *Neuron* **50**, 23–33 (2006).
6. Alilain, W.J. *et al.* Light-induced rescue of breathing after spinal cord injury. *J. Neurosci.* **28**, 11862–11870 (2008).
7. Aponte, Y., Atasoy, D. & Sternson, S.M. AGRP neurons are sufficient to orchestrate feeding behavior rapidly and without training. *Nat. Neurosci.* **14**, 351–355 (2011).
8. Atasoy, D., Aponte, Y., Su, H.H. & Sternson, S.M.A. FLEX switch targets channelrhodopsin-2 to multiple cell types for imaging and long-range circuit mapping. *J. Neurosci.* **28**, 7025–7030 (2008).
9. Cardin, J.A. *et al.* Driving fast-spiking cells induces gamma rhythm and controls sensory responses. *Nature* **459**, 663–667 (2009).
10. Gradinaru, V., Mogri, M., Thompson, K.R., Henderson, J.M. & Deisseroth, K. Optical deconstruction of parkinsonian neural circuitry. *Science* **324**, 354–359 (2009).
11. Haubensak, W. *et al.* Genetic dissection of an amygdala microcircuit that gates conditioned fear. *Nature* **468**, 270–276 (2010).
12. Kravitz, A.V. *et al.* Regulation of parkinsonian motor behaviours by optogenetic control of basal ganglia circuitry. *Nature* **466**, 622–626 (2010).
13. Sohal, V.S., Zhang, F., Yizhar, O. & Deisseroth, K. Parvalbumin neurons and gamma rhythms enhance cortical circuit performance. *Nature* **459**, 698–702 (2009).
14. Stuber, G.D., Hnasko, T.S., Britt, J.P., Edwards, R.H. & Bonci, A. Dopaminergic terminals in the nucleus accumbens but not the dorsal striatum corelease glutamate. *J. Neurosci.* **30**, 8229–8233 (2010).
15. Tsai, H.C. *et al.* Phasic firing in dopaminergic neurons is sufficient for behavioral conditioning. *Science* **324**, 1080–1084 (2009).
16. Witten, I.B. *et al.* Cholinergic interneurons control local circuit activity and cocaine conditioning. *Science* **330**, 1677–1681 (2010).

17. Cruikshank, S.J., Urabe, H., Nurmikko, A.V. & Connors, B.W. Pathway-specific feedforward circuits between thalamus and neocortex revealed by selective optical stimulation of axons. *Neuron* **65**, 230–245 (2010).
18. Varga, V. *et al.* Fast synaptic subcortical control of hippocampal circuits. *Science* **326**, 449–453 (2009).
19. Arenkiel, B.R. *et al.* In vivo light-induced activation of neural circuitry in transgenic mice expressing channelrhodopsin-2. *Neuron* **54**, 205–218 (2007).
20. Wang, H. *et al.* High-speed mapping of synaptic connectivity using photostimulation in Channelrhodopsin-2 transgenic mice. *Proc. Natl. Acad. Sci. USA* **104**, 8143–8148 (2007).
21. Tomita, H. *et al.* Visual properties of transgenic rats harboring the channelrhodopsin-2 gene regulated by the thy-1.2 promoter. *PLoS ONE* **4**, e7679 (2009).
22. Hagglund, M., Borgius, L., Dougherty, K.J. & Kiehn, O. Activation of groups of excitatory neurons in the mammalian spinal cord or hindbrain evokes locomotion. *Nat. Neurosci.* **13**, 246–252 (2010).
23. Dhawale, A.K., Hagiwara, A., Bhalla, U.S., Murthy, V.N. & Albeanu, D.F. Non-redundant odor coding by sister mitral cells revealed by light addressable glomeruli in the mouse. *Nat. Neurosci.* **13**, 1404–1412 (2010).
24. Chuhma, N., Tanaka, K.F., Hen, R. & Rayport, S. Functional connectome of the striatal medium spiny neuron. *J. Neurosci.* **31**, 1183–1192 (2011).
25. Sagne, C. *et al.* Cloning of a functional vesicular GABA and glycine transporter by screening of genome databases. *FEBS Lett.* **417**, 177–183 (1997).
26. Gasnier, B. The loading of neurotransmitters into synaptic vesicles. *Biochimie* **82**, 327–337 (2000).
27. Gunaydin, L.A. *et al.* Ultrafast optogenetic control. *Nat. Neurosci.* **13**, 387–392 (2010).
28. Qin, C. & Luo, M. Neurochemical phenotypes of the afferent and efferent projections of the mouse medial habenula. *Neuroscience* **161**, 827–837 (2009).
29. Bennett, B.D., Callaway, J.C. & Wilson, C.J. Intrinsic membrane properties underlying spontaneous tonic firing in neostriatal cholinergic interneurons. *J. Neurosci.* **20**, 8493–8503 (2000).
30. Vandermaelen, C.P. & Aghajanian, G.K. Electrophysiological and pharmacological characterization of serotonergic dorsal raphe neurons recorded extracellularly and intracellularly in rat brain slices. *Brain Res.* **289**, 109–119 (1983).
31. Liu, R.J., Lambe, E.K. & Aghajanian, G.K. Somatodendritic autoreceptor regulation of serotonergic neurons: dependence on L-tryptophan and tryptophan hydroxylase-activating kinases. *Eur. J. Neurosci.* **21**, 945–958 (2005).
32. Lee, S.H., Govindaiah, G. & Cox, C.L. Heterogeneity of firing properties among rat thalamic reticular nucleus neurons. *J. Physiol. (Lond.)* **582**, 195–208 (2007).
33. Huguenard, J.R. & Prince, D.A. A novel T-type current underlies prolonged Ca(2+)-dependent burst firing in GABAergic neurons of rat thalamic reticular nucleus. *J. Neurosci.* **12**, 3804–3817 (1992).
34. Llinas, R. & Sugimori, M. Electrophysiological properties of in vitro Purkinje cell dendrites in mammalian cerebellar slices. *J. Physiol. (Lond.)* **305**, 197–213 (1980).
35. Katzel, D., Zemelman, B.V., Buetfering, C., Wolfel, M. & Miesenbock, G. The columnar and laminar organization of inhibitory connections to neocortical excitatory cells. *Nat. Neurosci.* **14**, 100–107 (2011).
36. Madisen, L. *et al.* A robust and high-throughput Cre reporting and characterization system for the whole mouse brain. *Nat. Neurosci.* **13**, 133–140 (2010).

ONLINE METHODS

Resource availability. The cell type–specific *ChR2(H134R)-EYFP* BAC transgenic mouse lines developed in this study have been deposited to the Jackson Laboratory and are under development for future distribution. The stock names, numbers and links to the Jackson Laboratory strain info web pages are: *VGAT-ChR2(H134R)-EYFP* stock number 014548 B6.Cg-Tg(Slc32a1-COP4*H134R/EYFP)8Gfng/J (http://jaxmice.jax.org/strain/014548.html); *ChAT-ChR2(H134R)-EYFP* line 6 stock number 014546 B6.Cg-Tg(Chat-COP4*H134R/EYFP)6Gfng/J (http://jaxmice.jax.org/strain/014546.html); *ChAT-ChR2(H134R)-EYFP* line 5 stock number 014545 B6.Cg-Tg(Chat-COP4*H134R/EYFP)5Gfng/J (http://jaxmice.jax.org/strain/014545.html); *TPH2-ChR2(H134R)-EYFP* (stock number 014555 B6;SJL-Tg(Tph2-COP4*H134R/EYFP)5Gfng/J (http://jaxmice.jax.org/strain/014555.html); and *Pvalb-ChR2(H134R)-EYFP* stock number 012355 B6;SJL-Tg(Pvalb-COP4*H134R/EYFP)15Gfng/J (http://jaxmice.jax.org/strain/012355.html).

Antibodies. Rabbit antibody to GFP (anti-GFP; A11122, 1:1,000 dilution) was from Invitrogen, mouse antibody to GFP (anti-GFP; Mab3580, 1:1,000 dilution), mouse antibody to GAD67 (anti-GAD67; Mab5406, 1:1,000 dilution) and goat antibody to ChAT (anti-ChAT; AB144P, 1:200 dilution) were from Millipore. Mouse antibody to TPH2 (anti-TPH2; T0678, 1:500 dilution) was from Sigma. Rabbit antibody to parvalbumin (anti-Pvalb; PV-28, 1:5,000 dilution) was from Swant.

Generation of cell type–specific *ChR2(H134R)-EYFP* BAC transgenic mice. The BAC transgenic mice were generated as previously described[37]. Briefly, BAC clones were obtained from Children's Hospital Oakland Research Institute. *ChR2(H134R)-EYFP* was engineered into the ATG exon of the specific BAC clones through homologous recombination (**Supplementary Fig. 1** and **Supplementary Table 1**). Transgenic mice were generated by the injection of modified BAC DNA constructs into fertilized oocytes, using standard pronuclear injection techniques[38]. Fertilized eggs were collected from matings between C57BL/6J and CBA F1 hybrids. Genotypes were determined by PCR from mouse tail DNA samples (**Supplementary Table 3**). Mice with the transgene were kept as founders to establish transgenic lines by mating to C57BL/6J mice. All research involving mice was conducted according to the Institutional Animal Care and Use Committee guidelines at Duke University. All procedures were approved by the Institutional Animal Care and Use Committee at Duke University.

Section preparation and imaging. Mouse brain section and imaging were done as previously described[37]. Briefly, mice were anesthetized by the inhalation of isoflurane and were intracardially perfused with Lactated Ringer's solution, followed by fixation in 4% paraformadehyde. Mouse brains were then fixed in 4% paraformadehyde overnight at 4 °C. Using a vibratome, 50 µm sagittal or coronal sections were cut, then mounted and imaged with a Zeiss AxioImager A1 microscope using a 5× objective or with Nikon PCM2000 confocal microscope using a 20× objective. Rabbit or mouse anti-GFP was used in co-immunostaining with anti-GAD67, anti-ChAT, anti-TPH2 or anti-Pvalb. Briefly, sections were blocked with blocking buffer (5% (vol/vol) normal goat serum, 2% (wt/vol) BSA and 0.2% (vol/vol) Triton X-100 in PBS) (0.1 M Tris, pH 7.6, was used for anti-GAD67 and anti-ChAT) for 1 h at room temperature (23–25 °C), then incubated with primary antibody overnight at 4 °C. After incubation with the primary antibody, sections were washed with either PBS or 0.1 M Tris three times every 20 min, followed by incubation with Alexa Fluor 488– or Cy3-conjugated secondary antibodies for 2–4 h at room temperature and then washed with PBS or 0.1 M Tris. Sections were transferred onto slides, dried, mounted with 0.1% paraphenylinediamine in 90% (wt/vol) glycerol-PBS (PPD) and imaged with a Nikon PCM2000 confocal microscope.

Equipment and settings. The montage images of the mouse brain sagittal or coronal sections in **Supplementary Figures 2a**, **3**, **6a**, **7**, **12a** and **14a** were taken with the Zeiss AxioImager A1 microscope equipped for fluorescence with a FITC filter and an AxioCamHR camera. The software used was AxioVision Rel 4.7 with the following main settings: 5×–1× tube, X-scaling: 1.275 µm per pixel, Y-scaling: 1.275 µm per pixel, frame-pixel-distance 6.45. The exposure time was 100–200 ms. The montage images were adjusted for brightness and contrast in Photoshop and converted from RGB to CMYK mode.

The confocal images in **Supplementary Figures 2b–d**, **6b–d**, **12b–d** and **14b**,**c** were taken on a Nikon PCM2000 confocal microscope. The objective lens used was 20×, 0.75 DIC M. The main settings were: large pinhole; first dichroic slider, RGB-red, 505-green; second dichroic slider, 565 for both red and green fluorescence images; ND filter selector, 10% transmission. The software used was Simple PCI 4.06 with the following settings: capture mode, 2× integration; fast scan mode, 1× fast scan; color, PCM2000 1024 color; PMT black level, 350; PMT gain, 1,000–1,500. The confocal TIFF files were equally adjusted for brightness and contrast in Photoshop and cropped to 500 × 500 pixels. Red color was converted to magenta, and the image was converted to CMYK mode.

Acute brain-slice preparation and electrophysiology. Acute brain slices were prepared from predominantly mature adult (2–8 months) mice but in some limited cases (for example, brainstem slices from *TPH2-ChR2(H134R)-EYFP* mice) from juvenile (21–30–day-old) mice according to our recently reported modified adult brain slice methodology[39] but with a few additional improvements. The mice were deeply anesthetized by intraperitoneal injection of tribromoethanol (Avertin) and then transcardially perfused with 25–30 ml of carbogenated protective artificial cerebrospinal fluid (aCSF) of the following composition: 92 mM *N*-methyl-D-glucamine (NMDG), 2.5 mM KCl, 1.25 mM NaH_2PO_4, 30 mM $NaHCO_3$, 20 mM HEPES, 25 mM glucose, 2 mM thiourea, 5 mM Na-ascorbate, 3 mM Na-pyruvate, 0.5 mM $CaCl_2{\cdot}4H_2O$ and 10 mM $MgSO_4{\cdot}7H_2O$. The pH of the solution was titrated to 7.3–7.4 with concentrated HCl (which provides Cl^- counter-ions for NMDG). HEPES and thiourea plus ascorbate were included as critical components to reduce edema and oxidative damage during slicing, recovery and extended slice incubation[40,41]. Mice were then decapitated, and the brains were removed into the cutting solution for an additional 1 min. The brains were then rapidly embedded in 2% low-melt agarose and mounted for either coronal (cortex, hippocampus, olfactory bulb, brain stem and medial habenula (MHb) or sagittal (cerebellum)

sectioning at 300 µM thickness on a VF200 model Compresstome (Precisionary Instruments) using a zirconium ceramic injector style blade (Specialty Blades). Acute brain slices containing the habenulo-peduncular pathway were prepared using a special slicing angle of 55–60° off the horizontal axis as shown in **Supplementary Figure 10a** and as described recently[42]. For midbrain slices containing the DRN the slice thickness was reduced to 200 µM to improve visualization using IR-DIC optics.

Slices were initially recovered for ≤20–30 min at room temperature (23–25 °C) in carbogenated protective cutting aCSF. In later experiments we refined the procedure by performing this initial recovery at 32–34 °C for ≤10–15 min rather than at room temperature, which we found provided improved visualization. The exact duration of the recovery period was critical for obtaining the optimal balance between morphological and functional preservation of the brain slices, and the timing of this recovery step exhibited clear temperature dependence, as indicated above based on extensive empirical testing. Proper implementation of this brief protective recovery step using our NMDG-based aCSF formula greatly reduced initial neuronal swelling during rewarming and enabled routine preparation of healthy acute brain slices for targeted whole-cell recordings from mature adult and aging mice. After this initial recovery period the slices were transferred into a holding chamber containing room-temperature carbogenated aCSF of the following composition: 119 mM NaCl, 2.5 mM KCl, 1.25 mM NaH_2PO_4, 26 mM $NaHCO_3$, 12.5 mM glucose, 2 mM $CaCl_2{\cdot}4H_2O$ and 2 mM $MgSO_4{\cdot}7H_2O$. The aCSF was supplemented with 2 mM thiourea, 5 mM Na-ascorbate and 3 mM Na-pyruvate to improve slice health and longevity, and slices were stored for 1–5 h before transfer to the recording chamber for use. The osmolarity of all solutions was measured at 300–310 mOsm and the pH was maintained at ~7.3 after equilibration under constant carbogenation. In some experiments using juvenile mice, the slices were cut using standard methods (standard aCSF instead of NMDG-based aCSF for cutting and recovery). Although the slice quality was deemed to be inferior based on morphological appearance and ease of identifying cells for targeted recordings, the experimental results obtained using this standard method with juvenile mice were indistinguishable and thus were pooled.

The slices were transferred one at a time to the recording chamber of a BX51WI microscope (Olympus) equipped with infrared DIC optics (900 nm) and epifluorescence. The slices were constantly perfused with room-temperature (22–25 °C) carbogenated recording aCSF at a rate of 4 ml min^{-1}. Whole-cell patch-clamp recordings were obtained from visually identified neurons using borosilicate glass pipettes (King Precision Glass; glass type 8250) pulled on a horizontal pipette puller (P-87, Sutter Instruments) to a resistance of 3–4 MΩ when filled with the internal solution containing 145 mM K-gluconate, 10 mM HEPES, 1 mM EGTA, 2 mM Mg-ATP, 0.3 mM Na^2-GTP and 2 mM $MgCl_2$. The pH was adjusted to 7.3 with KOH and the osmolarity was adjusted to 290–300 mOsm with sucrose. This internal composition was selected to more readily distinguish spontaneous and light-evoked inhibitory synaptic events as clear outward currents at a holding potential of −50 mV or −60 mV in voltage clamp mode. The reversal potential for Cl^- was experimentally determined to be −75 mV. The theoretical liquid junction potential was calculated at −11 mV and was not corrected.

Neurons expressing ChR2 were identified by visualization of membrane-targeted EYFP fluorescence around the somata of genetically labeled neuron types. A holding command of −60 mV (except where indicated) was applied to the patched cell, and once the whole-cell mode was established the cell was allowed to stabilize for 2–5 min. Blue laser light (473 nm) was delivered through a 200-µm-diameter optic fiber (Thor Labs) positioned at the slice surface over the recorded neuron. The other end of the optic fiber was coupled to a commutator and then to the laser (Crystal Laser, 100 mW) and the laser power was controlled by an analog dial. The illuminated area was estimated as a 400 µm by 600 µm oval (0.24 mm^2) and this area was used to calculate the power density following direct measurement of the power output at the optic fiber tip using a power meter (Thor Labs). Pulsing of the laser was computer-controlled using custom 'optogenetics' stimulation protocols designed in the pClamp 10.2 software. Light-induced inward currents were evoked with blue laser light delivered at 1–100 Hz frequencies (0.05–5 ms pulse duration), or by continuously applying blue laser light over 1 s or longer. Similar protocols were applied in the current clamp mode to monitor action potential firing of the recorded neurons in response to blue-light stimulation from the resting membrane potential. For tonically active neurons (often seen for striatal cholinergic neurons, cerebellar Purkinje cells and DRN serotonergic neurons) we assessed the ability to induce action potential firing either on top of basal firing rates or after silencing basal firing with the minimal necessary hyperpolarizing current injection. For experiments using *VGAT-ChR2(H134R)-EYFP* brain slices to assess ChR2-mediated silencing in local circuits, a layer V cortical neuron was recorded in whole-cell current clamp mode and injected continuously with 100–200 pA of depolarizing current to induce tonic firing. Blue laser light was applied to nearby ChR2-expressing cortical interneurons to assess the extent of silencing or hyperpolarization in the layer V pyramidal neuron. Cell-attached recordings were performed in some experiments to monitor action-potential firing without disruption of the cytosol. Cell-attached recordings were performed in voltage clamp mode with a zero holding current. Extracellular field recordings were obtained by placement of a glass recording electrode (1–2 MΩ tip) filled with aCSF into the slice and advanced to the depth that allowed discrimination of putative single units based on the response to blue laser light stimulation (in some cases multiple units were apparent).

A Multiclamp 700B amplifier (Molecular Devices Corporation) and Digidata 1440A were used to acquire electrophysiological signals using Clampex 10.2 software (Molecular Devices). The signals were sampled at 20 kHz and low-pass filtered at 2 kHz. The series resistance was ≤ 25 MΩ and was not compensated. Access to the recorded cells was continuously monitored, and only recordings with stable series resistance were included for analysis. All data analysis was performed using Clampfit 10.2 software. Values are expressed as mean ± s.e.m. Data were tested for significance using a nonpaired student *t*-test.

Additional acute brain slice electrophysiological recordings were conducted in the Luo laboratory using previously published procedures with only minor modification[42].

***In vivo* electrophysiology.** Mice were deeply anaesthetized with isoflurane and fitted with light-weight head stages for chronic

doi:10.1038/nmeth.1668

recording with multiple tetrodes in the mouse striatum[43,44] (Specialty Machining). A small opening in the skull and corresponding incision of the dura mater were made to allow entry of seven tetrodes (each made up of twisted 10 µm Ni-Cr wires) and one fiberoptic cable (100–125 µm, attached to a 1.25-mm ferrule) into the brain parenchyma. Both the tetrodes and the fiber optic cable were held individually in a series of nested polyimide tubes. The tubes, attached to microdrives, were held parallel to screws that were used to advance independently each tetrode and the fiber. After the mice recovered for a week after surgery, the tetrodes and the fiber optic cable were lowered, day by day, through the full dorso-ventral extent of the anterior striatum (anterior-posterior +1.5 mm, medial-lateral +1.2 mm, dorsal-ventral +1.9–3.3 mm) and recordings and stimulation sites were arranged along these trajectories. The tip of the fiberoptic cable was kept 0.5 mm above the tips of the tetrodes.

During neuronal recording sessions, a 16-channel preamplifier (1.7 g) connected to lightweight wires (Neuralynx) was attached to the headstage. Neuronal activity recorded on each tetrode channel was sent through the preamplifier with unity gain to two 8-channel programmable amplifiers (gain, 2,000–10,000 times; filter, 0.6–6 kHz) and then to a Cheetah data-acquisition system (Neuralynx). The spike waveform of each spike was digitized at 32 kHz and stored with a microsecond-precision time stamp. The fiber optic cable was coupled to a 473 nm laser (100 mW, Shanghai Dream Lasers) by connecting its ferrule to the ferrule at the end of the fiber optic cable attached to the laser. A Zirconia sleeve (Doric Lenses) was used to couple the two ferrules. The laser was controlled by a TTL circuit connecting it to a computer running Delphi software. TTL pulses were concurrently sent to the Cheetah data-acquisition system where they received a time stamp and were stored. Laser power was measured before each session through the fiberoptic cable that connected the laser to the head stage fiber. The mouse was placed in a circular container (20 cm diameter) for the recording sessions and was allowed to move freely. Typically, each session consisted of 16 trials (40 s each) during which laser-on and laser-off trials were interleaved and separated by a 1 minute gap. The tetrodes and the fiber optic cable were moved between sessions to maximize the number of unique neurons recorded.

Unit activity containing the spikes of multiple neurons was sorted off-line into putative single units (clusters) according to multiple spike parameters (for example, peak height, valley depth, peak time) on the four channels of each tetrode (DataWave Technologies). The accuracy of spike-sorting and the quality of the single units were then evaluated by (i) *t*-test for spike variability, (ii) spike waveform overlays to confirm uniform waveforms for a given unit and different waveforms across units and (iii) autocorrelograms to detect the presence of an absolute refractory period. Based on these tests, clusters containing noise (artifacts and the activity of other units) were excluded from further analyses. All accepted units were classified as putative MSNs, fast-firing interneurons or tonically active interneurons based on properties of discharge patterns identified by calculating interspike intervals, autocorrelograms and firing rates[45]. MSNs that fired fewer than 150 spikes in a session were not included in any analysis. Histograms are displayed in bins of variable sizes time-locked to the first laser pulse for laser-on trials and the beginning of recording for laser-off trials. The order of trials was interleaved (on, off, on, off and so on) and the trials were separated by 1 min. A paired *t*-test was performed to determine statistical significance of the firing rate change between laser-on and laser-off trials.

37. Zhao, S. *et al.* Fluorescent labeling of newborn dentate granule cells in GAD67-GFP transgenic mice: a genetic tool for the study of adult neurogenesis. *PLoS ONE* **5**, e12506 (2010).
38. Feng, G. *et al.* Imaging neuronal subsets in transgenic mice expressing multiple spectral variants of GFP. *Neuron* **28**, 41–51 (2000).
39. Peca, J. *et al.* Shank3 mutant mice display autistic-like behaviours and striatal dysfunction. *Nature* **472**, 437–442 (2011).
40. Brahma, B., Forman, R.E., Stewart, E.E., Nicholson, C. & Rice, M.E. Ascorbate inhibits edema in brain slices. *J. Neurochem.* **74**, 1263–1270 (2000).
41. MacGregor, D.G., Chesler, M. & Rice, M.E. HEPES prevents edema in rat brain slices. *Neurosci. Lett.* **303**, 141–144 (2001).
42. Ren, J. *et al.* Habenula "cholinergic" neurons corelease glutamate and acetylcholine and activate postsynaptic neurons via distinct transmission modes. *Neuron* **69**, 445–452 (2011).
43. Jog, M.S. *et al.* Tetrode technology: advances in implantable hardware, neuroimaging, and data analysis techniques. *J. Neurosci. Methods* **117**, 141–152 (2002).
44. Kubota, Y. *et al.* Stable encoding of task structure coexists with flexible coding of task events in sensorimotor striatum. *J. Neurophysiol.* **102**, 2142–2160 (2009).
45. Barnes, T.D., Kubota, Y., Hu, D., Jin, D.Z. & Graybiel, A.M. Activity of striatal neurons reflects dynamic encoding and recoding of procedural memories. *Nature* **437**, 1158–1161 (2005).